PROCEEDINGS B

royalsocietypublishing.org/journal/rspb

Research

Cite this article: Adhikari P, Uprety S, Feigl B, Zele AJ. 2024 Melanopsin-mediated amplification of cone signals in the human visual cortex. *Proc. R. Soc. B* **291**: 20232708. https://doi.org/10.1098/rspb.2023.2708

Received: 30 November 2023
Accepted: 2 May 2024

Subject Category:
Neuroscience and cognition

Subject Areas:
behaviour, cognition, neuroscience

Keywords:
melanopsin, cones, vision, visual evoked potentials, electroretinogram

Author for correspondence:
Andrew J. Zele
e-mail: andrew.zele@qut.edu.au

THE ROYAL SOCIETY PUBLISHING

Melanopsin-mediated amplification of cone signals in the human visual cortex

Prakash Adhikari[1], Samir Uprety[1], Beatrix Feigl[1,2,3] and Andrew J. Zele[1]

[1]Centre for Vision and Eye Research, and [2]School of Biomedical Sciences, Queensland University of Technology (QUT), Brisbane, Queensland 4059, Australia
[3]Queensland Eye Institute, Brisbane, Queensland 4101, Australia

PA, 0000-0003-4834-8500; BF, 0000-0001-7198-7373; AJZ, 0000-0003-0291-9929

The ambient daylight variation is coded by melanopsin photoreceptors and their luxotonic activity increases towards midday when colour temperatures are cooler, and irradiances are higher. Although melanopsin and cone photoresponses can be mediated via separate pathways, the connectivity of melanopsin cells across all levels of the retina enables them to modify cone signals. The downstream effects of melanopsin-cone interactions on human vision are however, incompletely understood. Here, we determined how the change in daytime melanopsin activation affects the human cone pathway signals in the visual cortex. A 5-primary silent-substitution method was developed to evaluate the dependence of cone-mediated signals on melanopsin activation by spectrally tuning the lights and stabilizing the rhodopsin activation under a constant cone photometric luminance. The retinal (white noise electroretinogram) and cortical responses (visual evoked potential) were simultaneously recorded with the photoreceptor-directed lights in 10 observers. By increasing the melanopsin activation, a reverse response pattern was observed with cone signals being supressed in the retina by 27% ($p = 0.03$) and subsequently amplified by 16% ($p = 0.01$) as they reach the cortex. We infer that melanopsin activity can amplify cone signals at sites distal to retinal bipolar cells to cause a decrease in the psychophysical Weber fraction for cone vision.

1. Introduction

Between dawn and dusk, the melanopsin-expressing intrinsically photosensitive retinal ganglion cells (ipRGC), rod and three cone photoreceptor classes are active in humans. During these daylight hours, melanopsin activation increases towards midday when colour temperatures are cooler, and illuminations are higher. Through ipRGC projections to the visual cortex via the dLGN [1,2], preferential stimulation of melanopsin evokes haemodynamic responses in area V1 [3] and conscious visual perception [3–9]. To provide a unified visual percept during continual changes in the spectral power distribution of the environmental light, the visual system is therefore tasked with merging signals from the melanopsin and cone pathways having distinct spectral, spatial and temporal contrast responses. It is the convergence of cone and melanopsin signals that changes the behaviour of retinal circuits and potentially, at downstream post-retinal sites to affect visual functions. These downstream processes are not however well understood and are investigated here.

With higher levels of melanopsin excitation, the photopic cone-directed electroretinogram (ERG), as an index of the function of outer retinal cells, shows a suppression of the b-wave amplitude that is near-synchronous with the melanopsin activation [10–12]. Such inhibitory retinal interactions are thought to be mediated via retrograde signals between the ipRGCs and the outer retina [13,14]. Conversely, cone-mediated visual contrast sensitivity can increase with higher levels of melanopsin excitation [5,15,16], indicating that the

suppressed retinal signals are amplified, with the site yet to be defined. To identify the cortical contribution to this interaction, we explore whether melanopsin activity can differentially modulate retinal and cortical signals to set cone-mediated visual sensitivity.

Most of our knowledge on how melanopsin shapes cone-mediated human processes is from ERG [10,17] and psychophysical studies [15,16,18,19] implementing sophisticated photoreceptor silent substitution protocols, with some approaches leaving the rod activation level uncontrolled. The significance of leaving rod excitations unrestrained is that melanopsin-directed stimulations inadvertently introduce concomitant rod intrusions due to overlapping melanopsin and rod spectral responses. In photopic lighting, mammalian rods can escape saturation [20–23] and interact with both cone [24] and melanopsin signals [16]. Given that the photopic rod-melanopsin [16] and cone-melanopsin interactions [5,15,16] can be of opposite polarity, the melanopsin enhancement of cone contrast sensitivity may be of lower magnitude [15] or completely nulled depending on the level of rod intrusion if it is left uncontrolled [18]. We therefore apply a custom-developed 5-primary spectral tuning method to silence rhodopsin while varying the melanopsin activation level. A full-field white noise electrophysiological technique simultaneously probes cone-directed retinal and cortical visual evoked responses (VEPs) at a constant photopic luminance. With this approach, we predict that the change in daylight melanopsin activity can differentially modify the cone-directed responses at early (outer retinal) and later (post-bipolar cell/cortical) sites within the intact, human visual system.

2. Material and methods

(a) Participants and ethics statement

All experimental protocols were approved and carried out in accordance with the Queensland University of Technology (QUT) Human Research Ethics Committee approval (no. 1700000699) and followed the tenets of the Declaration of Helsinki; written informed consent was obtained by the authors from all participants. All 10 participants (3 females, 7 males; 29–47 years) had visual acuity of 0.0 logMAR (6/6) or better, age-normal spatial contrast sensitivity (Spatial Contrast Vision Chart) [25], trichromatic colour vision (Ishihara pseudoisochromatic plates and L'anthony Desaturated D-15 Test), no ocular diseases as confirmed with ophthalmoscopy, optical coherence topography (RS-3000 OCT RetinaScan Advance, Nidek Co., Tokyo, Japan), fundus photography (Canon Non Mydriatic Retinal Camera, CR-DGi, Canon Inc., Tokyo, Japan) and intraocular pressure measurement (less than 21 mmHg) (Icare ic100; Icare Finland Oy, Vantaa, Finland), and no systemic disease.

(b) Apparatus

A custom-built 5-primary monocular Ganzfeld apparatus was developed to spectrally tune the full-field retinal illumination with independent control of all five photoreceptor excitations using the method of silent substitution [26,27]. A gamut suitable for complete photoreceptor control [28] was generated with five narrowband LED and interference filter combinations (Thorlabs, Newton, NJ, USA) with peak wavelengths (full width at half maximum) at 449 nm (15 nm) for the blue (B) primary, 497 nm (10 nm) for the cyan (C), 547 nm (25 nm) for the green (G), 593 nm (13 nm) for the amber (A) and 654 nm (13 nm) for the red (R). The 5-primary light outputs were modulated using an LED driver (TLC5940), microcontroller (Arduino Uno SMDR3, Model A000073), and custom designed software (Xcode 3.2.3, 64-bit, Apple, Inc., Cupertino, CA, USA) having 12-bit resolution and a high frequency limit of 488 Hz [5].

To assess the effect of melanopsin on cone pathway signals, the retinal wnERG and cortical wnVEP were simultaneously recorded using an Espion E2 system (Colordome; Diagnosys, Lowell, MA, USA) at a sampling rate of 1000 Hz and filtered between 0.3 and 300 Hz in accordance with the International Society for Clinical Electrophysiology of Vision (ISCEV) guidelines [29]. The protocol was triggered by an Apple MacPro QuadCore Intel computer, which controlled the trigger input to start the silent substitution protocol and ERG/VEP recording via a microcontroller (Arduino Uno SMD R3, Model A000073). System delays were accounted for during *post hoc* analyses.

(c) Experimental design: photoreceptor spectral tuning protocols

For silent substitution, the physical light outputs and individual observer calibrations were performed in accordance with standardized protocols [27]. The photoreceptor-directed lights were specified initially with reference to the CIE 1964 10° standard observer cone spectral sensitivities, rhodopsin nomogram and melanopsin nomogram [30]. Because the spectral responses of rhodopsin and melanopsin are positively correlated [31], the maximum 59.6% melanopsin Weber contrast at the adapting chromaticity (1964 CIE$x,y = 0.549$, 0.410) would introduce a concomitant 43.0% rod Weber contrast intrusion if rhodopsin was not controlled in our silent substitution protocol [27,32]. Non-visual opsins identified in mammals, including humans, such as OPN3, OPN5 and a retinal G protein-coupled receptor, are not considered in this silent-substitution protocol due to a lack of direct evidence for any light-dependent role in human image-forming functions [27].

Individual observer calibrations were performed using heterochromatic flicker photometry (HFP) [33] to determine the scaling factors required to correct for individual deviations in pre-receptoral filtering and photoreceptor spectral sensitivity from the CIE standard observer functions [27]. The instrument gamut was maximized with an orange-appearing adaptation background ($l = 0.752$, $s = 0.105$ and $r = 0.319$; 1964 CIE $x = 0.549$, $y = 0.410$) that differed by 52.6% (Weber contrast) between a lower and higher melanopsin excitation ($i_{low} = 0.19$ and $i_{high} = 0.29$) designed to intentionally envelope a broad range of the total daytime variation in melanopsin activity [34]. We changed the background melanopsin excitation independently of the cone and rhodopsin excitations at a fixed photometric luminance (159.2 cd m^{-2}). We could therefore specify the cone-mediated electrophysiological responses with reference to the circadian equivalent daytime variation in melanopsin excitation (biological efficacy). This daytime variation of melanopsin is non-linearly related to the correlated colour temperature [34] and for our experimental conditions, varies between a lower (1645K; delta $u,v = 0.0029$) and higher state (1955K; delta $u,v = 0.0039$). The lower state served as the control [4,18,35]. The cone-directed temporal white noise (TWN) stimuli [36,37] modulated the L-, M- and S-cone photoreceptor excitations (20% Michelson contrast) in the same phase to photoreceptor-directed (LMS) cone luminance noise without introducing a change in the rhodopsin and melanopsin excitations.

Our calculations show that the differential absorption of the primary lights by the open-field cones and the macular pigment [38] can introduce ≤ 0.1% undesired luminance (L+M) contrast and ≤ 0.4% chromatic (+L-M) contrast errors in both the low and high melanopsin adapting backgrounds, and ≤ 0.2% L+M contrast and ≤ 0.4% +L-M contrast errors in the cone-directed white noise stimulus. Penumbral cones in the shadow of the retinal vasculature [7,39] might present ≤ 0.3% L+M contrast and ≤ 0.6% +L-M contrast with the adapting backgrounds, and ≤ 0.3% L+M contrast and 0.8% +L-M contrast for the cone-directed stimulus. It is important to emphasize that we did not generate a melanopsin-directed stimulus; we implemented cone-directed stimuli under steady-state adaptation that had either a lower or higher melanopsin excitation. This means that the imperfections in the cone photoreceptor isolation will be similar magnitude between the two background states and simply add to the cone stimulus contrast, without confounding the interpretation of the effect of melanopsin on cone signals. As such, these measured contrast imperfections are smaller than can be detected in an ERG recording [10,37,40–43], and at such levels, their magnitude is too low to modify cone-mediated visual thresholds [19]. Accordingly, none of our observers reported the appearance of Maxwell's spot [44] or a Purkinje tree [39], with the orangish appearing background [44,45], and with the balanced rod activity across the central and peripheral visual field [46].

(d) Temporal white noise electrophysiology procedures

The electrodes were set-up according to the ISCEV protocol for ERG [47] and VEP recordings [29]. For the wnERG, an active fibre electrode (Diagnosys, Lowell, MA, USA) was placed across the lower conjunctiva. The ground (forehead) and reference (temple) gold (Ag/AgCl) cup electrodes (Diagnosys, Lowell, MA, USA) were filled with conductive gel (Aquasonic; Parker Laboratories, Fairfield, NJ, USA) and pressed firmly to adhere to the skin after the areas scrubbed with alcohol wipes and abrasive gel (Nuprep; D. O. Weaver & Co., Aurora, CO, USA). For the wnVEP, the gold cup scalp electrodes (Diagnosys, Lowell, MA, USA) were placed according to the international 10/20 system [29], positioned relative to the bony landmark on the skull between the anterior-posterior midline of nasion and inion. The active electrode was placed on the midline sagittal plane of the occipital scalp over the visual cortex (Oz); the reference electrode was placed over the frontal lobe (*Fz*), and a common ground electrode for both ERG and VEP recording was positioned at central vertex of the skull (C_z). Electrode impedance was always below 5 kΩ.

A TWN stimulation paradigm [10,37,48,49] was used to electrophysiologically probe signals measured under conditions of retinal equilibrium with spectral tuning. Each 1 s TWN stimulus epoch contained 1024 photoreceptor excitations evenly distributed in the 0 to 64 Hz frequency range within a Gaussian distribution centred around the constant photopic adaptation level, with the phase varied randomly between 0° and 359°. The inverse fast Fourier transform of the TWN stimuli returns a constant amplitude spectrum in the 0 and 64 Hz temporal frequency range. To de-correlate the line frequency from the fundamental frequency of the stimulus and improve the signal to noise ratio of the averaged signal, each 1 s stimulus epoch was separated by a 1 ms blank interval set to the mean luminance and chromaticity [50]; the noise sequence was repeated to create 120 unique signal recordings during a total 120.12 s recording sequence. Each experimental condition was repeated twice so that all conditions had a minimum of 120 recordings per observer after artefact and blink removal. Electrophysiological signals were filtered to remove artefacts induced by blinks and large eye movements. The impulse response function (IRF) was derived by cross-correlating the TWN stimulus sequence with the filtered electrophysiological wnERG and wnVEP responses using custom-written MATLAB software (R2022b; Mathworks, Natick, MA, USA). To maximize the SNR, the noise stimuli and ERG/VEP response were time locked using circular cross correlation [51,52]. This method offers an advantage over a flash ERG in that the entire recording sequence can be used for analysis in the form of frequency distributions.

(e) General procedure

Stimuli were presented to the right eye in Newtonian view through the 3.81 cm Ganzfeld aperture. The pupil of the test eye was dilated (Tropicamide 1%; Bausch and Lomb, Australia; ≥ 8 mm diameter; 8000 Td). Following the electrode setup, participants underwent a 10 min dark adaptation. Prior to the presentation of the cone noise sequence, participants underwent preadaptation to either the low or high melanopsin adapting background to ensure recovery of melanopsin phototransduction from the onset of the background [35,53]. The order of presentation of the low and high melanopsin conditions was randomized. Between consecutive noise sequences, participants rested in the darkened laboratory. Recordings were performed at similar times to minimize the impact of circadian-dependent variation on melanopsin-mediated function [54].

(f) Data analysis

All statistical analyses were conducted using GraphPad Prism (GraphPad Software, Inc., CA, USA). The data frequency distributions were estimated using the D'Agostino and Pearson omnibus normality test. The wnERG and wnVEP amplitudes and implicit times are reported as the mean ± s.e.m calculated across 10 observers. To detect the difference in the LMS-cone directed response between low melanopsin (i_{low}) and high melanopsin (i_{high}) excitations (figure 1), the wnERG and wnVEP amplitudes, implicit times and coefficient of variation (CoV) were compared using paired *t*-test (normally distributed data) or Wilcoxon test (non-normally distributed data) (95% confidence interval, $p < 0.05$). If there is no melanopsin-cone interaction, the LMS cone-directed ERG (N1P1) and VEP (N2P2) amplitudes will be equal between i_{low} and i_{high} (figure 1). If melanopsin enhances cone signals, the amplitudes will be higher with i_{high} than with i_{low}. In the case of suppression, the amplitudes will be lower with i_{high} than with i_{low}. Because the ERG and VEP signals originate from different neurones (figure 1), we calculated the ratio of the cone IRF amplitudes between the two melanopsin states (i_{high}/i_{low}) for each observer to determine how melanopsin adaptation affects the total relative change in cone signals reaching the cortex (VEP) from those originally generated in the retina (ERG). The initial VEP component (e.g. N2 in our waveforms) is most likely generated in the thalamocortical radiations [55] and striate cortex (Brodmann's area 17, V1), with the later component (e.g. P2 in our waveforms) arising from the extrastriate cortex (Brodmann's areas 18 (V2) and 19 (V3, V4 and V5); for review, see [56]), indicating that the N2P2 amplitude is dominated by cortical activity. We therefore use the N2P2 amplitude as a biomarker of the primary visual cortical response (figure 1). We predict that the amplitude ratio (i_{high}/i_{low}) will be unity if there is no interaction, less than unity with suppression, and greater than unity with amplification. The ratios were then compared between the ERG and VEP using paired *t*-test (or Wilcoxon). To identify the presence of time-dependent effect of melanopsin adaptation, linear regression models were fitted to the wnERG and wnVEP amplitudes or implicit times recorded over time (120 recording epochs per observer). The optimal bin width for the frequency distributions of the electrophysiological recordings were determined based on the sample size and standard deviation [57] and modelled using a hyperbolic secant function. To determine

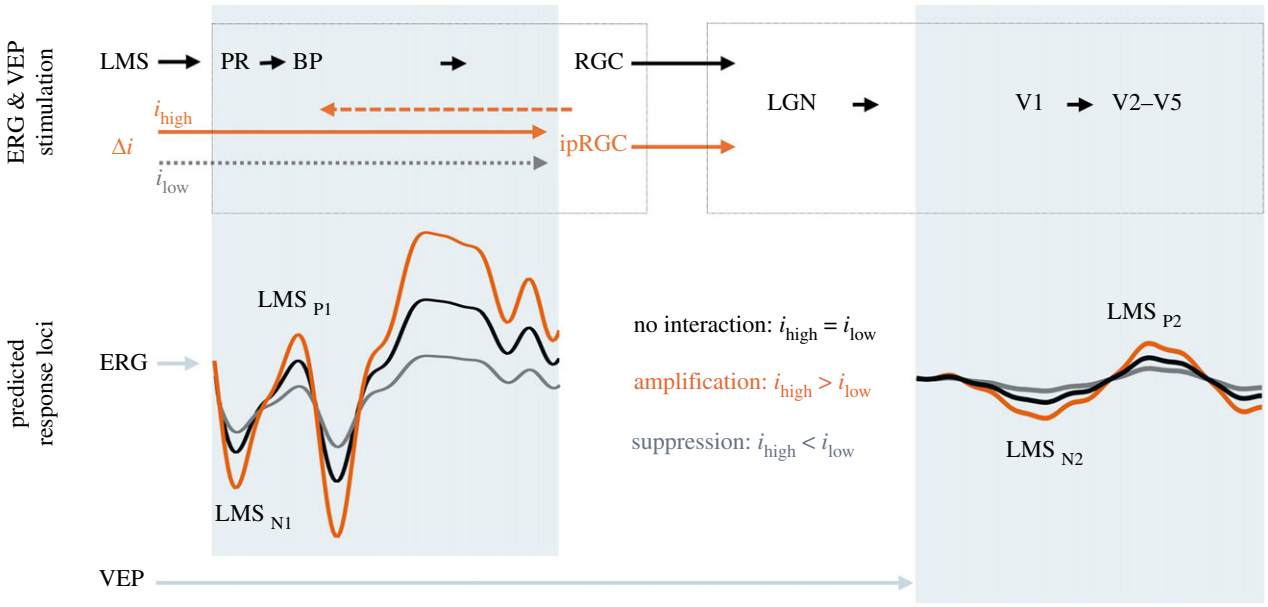

Figure 1. Predicted loci for the retinal (ERG waveforms) and cortical visual evoked potentials (VEP waveforms) recorded in response to cone-directed light stimulation (LMS) in the presence of lower (i_{low}) or higher (i_{high}) melanopsin excitation (Δi). The waveform predictions are with reference to the low melanopsin state, and the components (N1, P1, N2, P2) are aligned with their neural generators in the retina (ERG) and cortex (VEP). LMS cone pathway signalling is sequential from eye to brain (left to right, solid black arrows). Melanopsin ipRGCs feedforward (solid orange arrows, dotted grey arrow) and feedback (orange dashed arrow). PR, photoreceptors; BP, bipolar cells; RGC, retinal ganglion cells; ipRGC, intrinsically photosensitive RGCs; LGN, lateral geniculate nucleus; V1–5, visual areas 1–5.

whether melanopsin alters the coding efficiency of cone signalling, intra-observer coefficient of variation (CoV = s.d/mean) across the 120 epochs was calculated as a measure of signal to noise ratio.

3. Results

Our selection of a steady-state light adaptation protocol with five primaries (figure 2*a*: low melanopsin i_{low} background; figure 2*e*: high melanopsin i_{high} background) to completely specify all five photoreceptor excitations provides a clear separation of the effects of melanopsin and rhodopsin, with the high frequency, cone-directed white noise (wn) probe designed to limit intrusion from any abrupt temporal transient visual responses that occur with flash stimuli (figure 2*b*,*f*). Exemplar retinal wnERG (figure 2*c*,*g*) and cortical wnVEP (figure 2*d*,*h*) IRFs resemble the typical flash ERG and VEP, respectively; these were evident in all 10 observers.

In all 10 observers, the retinal IRF of the LMS-cone mediated wnERG (figure 3*c*) had an initial negative (N1) deflection at approximately11 ms (N1 implicit time: $i_{low} = 10.80 \pm 0.34$ ms; $i_{high} = 10.93 \pm 0.33$ ms; mean ± s.e.m.) followed by a positive (P1) deflection at approximately 39 ms (P1 implicit time: $i_{low} = 39.11 \pm 0.43$ ms; $i_{high} = 38.83 \pm 0.32$ ms). The cortical wnVEP (figure 3*d*) had a robust N2 component at approximately 65 ms (N2 implicit time: $i_{low} = 64.96 \pm 1.39$ ms; $i_{high} = 64.37 \pm 1.08$ ms) and P2 at ~101 ms (P2 implicit time: $i_{low} = 100.91 \pm 0.45$ ms; $i_{high} = 101.63 \pm 0.45$ ms). The mean wnERG and VEP metrics from each observer were used to evaluate the dependence of cone function on melanopsin excitation, independent of changes in rhodopsin and the photometric luminance. The high melanopsin excitation caused a statistically significant 27.13% reduction (Wilcoxon $W = -43.00$, $p = 0.03$) in the mean cone-directed N1P1 wnERG amplitude ($i_{low} = 384.84 \pm 39.41$ µV; $i_{high} = 280.45 \pm 43.30$ µV; mean ± s.e.m.; figure 3*a*) and a significant 16.08% increase ($t_9 = 3.67$, $p = 0.01$) in the cone-directed N2P2 wnVEP amplitude ($i_{low} = 92.53 \pm 15.41$ µV; $i_{high} = 107.21 \pm 14.04$ µV; figure 3*b*). All implicit times were invariant of the background melanopsin excitation (figure 3*c*,*d*).

As a metric of the magnitude of the melanopsin-cone interaction, the melanopsin-mediated cone suppression and amplification was defined as the amplitude ratio ($\mu i_{high}/\mu i_{low}$) of the mean cone IRF amplitude for each observer. In the retina, the wnERG amplitude ratio was less than unity (N1P1 = 0.74 ± 0.08) indicating that melanopsin supresses the wnERG amplitude (figure 4). When measured in the cortex, the wnVEP amplitude ratio was greater than unity (N2P2 = 1.24 ± 0.07), indicating that melanopsin amplifies the wnVEP. The wnERG amplitude ratio was significantly different from the wnVEP ratio ($t_9 = 6.02$, $p = 0.0002$). With reference to the suppressed retinal signals, the relative (total) amplification present in the cortex ($wnVEP_{N2P2\ ratio}/wnERG_{N1P1\ ratio}$) was therefore 1.84 ± 0.20. Ratios for implicit times were close to unity for both the wnERG (N1 = 1.01 ± 0.02; P1 = 0.99 ± 0.01) and wnVEP (N2 = 0.99 ± 0.01; P2 = 1.01 ± 0.00).

To determine whether the melanopsin signal can adapt the cone ERG [11] and VEP on the short timescales measured here, the 120 IRFs derived from each 2 min wnERG and wnVEP recording sequence for each observer were analysed as a function of adaptation time (figure 5) using regression. The linear regressions were not significantly different from zero for any observer and so all recordings from the 10 observers (at least 1200 total recordings and typically 1900 recordings) were pooled to determine the global effect of melanopsin adaptation. The linear regressions were not significantly different from zero (N1 amplitudes: i_{low}, $r^2 = 0.0009$, $F_{1,1949} = 1.92$, $p = 0.16$; i_{high} N1, $r^2 = 0.06$, $F_{1,2017} = 3.3$, $p = 0.06$; N1P1 amplitudes: i_{low}, $r^2 = 0.0008$, $F_{1,1949} = 1.52$, $p = 0.21$; i_{high}, $r^2 = 0.001$, $F_{1,2017} = 2.92$, $p = 0.08$), indicating that the IRFs of the wnERG did not significantly change during the short-term light

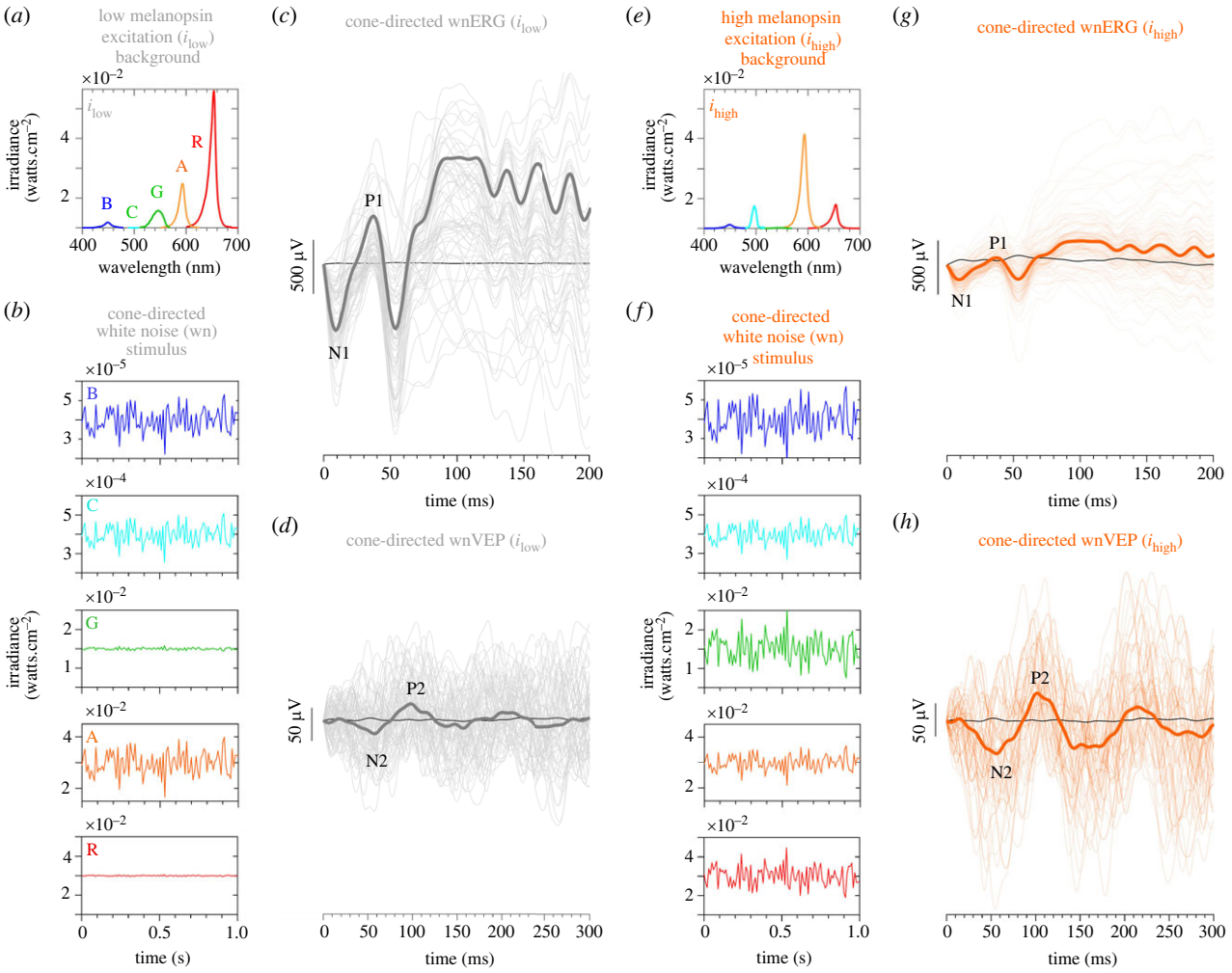

Figure 2. Retinal (wnERG) and cortical visual evoked potentials (wnVEP) recorded under conditions of photoreceptor silencing with lower (i_{low}) or higher (i_{high}) melanopsin excitations in the adapting background. (*a*) Spectral outputs of the 5-primary lights in the adapting background set to a melanopsin excitation having a low biological efficacy (i_{low}). (*b*) Temporal irradiance modulation of each of the five primaries (presented separately in five panels) required to generate an LMS cone-directed temporal white noise (wn) probe under the low melanopsin background (i_{low}), without changing rhodopsin. (*c*) Exemplar impulse response functions (IRF) of the cone-directed white noise electroretinogram (wnERG, grey lines) measured under low melanopsin excitation. Black line is the baseline recording (no white noise probe). (*d*) Exemplar visual cortical evoked potentials (wnVEP, grey lines) measured under low melanopsin excitation. (*e*) Spectral outputs of the primary lights in the adapting background to set the melanopsin excitation to a high biological efficacy (i_{high}). (*f*) Temporal irradiance modulation of each of the five primary spectra to generate an LMS cone-directed white noise probe at a high melanopsin excitation (i_{high}). (*g*) Exemplar cone-directed wnERG and (*h*) wnVEP measured under high melanopsin excitation (orange lines). The high and low melanopsin adaptation states (*a*,*e*) are equivalent for rods (i.e. rods silenced) and have a constant photometric luminance. To achieve the same LMS-cone temporal white noise stimulus contrast and amplitude pattern, and photometric luminance at both the low melanopsin (*b*) and high melanopsin (*f*) backgrounds, the 5-primaries have the same temporal noise amplitude patterns in the silent-substitution, but with different absolute irradiances to compensate for the different primary irradiance levels at the two backgrounds.

adaptation (figure 5*a*). The wnVEP responses also did not significantly change during the 2 min light adaptation (N2P2 amplitudes: i_{low}, $r^2 = 0.001$, $F_{1,1895} = 2.41$, $p = 0.12$; i_{high}, $r^2 = 0.001$, $F_{1,1895} = 1.74$, $p = 0.18$) (figure 5*b*).

The absence of short-term retinal adaptation (figure 5) allowed us to determine the global effect of melanopsin on cone responses by plotting the frequency distributions of the retinal and cortical IRF data (pooled data from figure 5). The distributions were sampled in their optimal bin width and described using the best-fitting hyperbolic secant function because of their positive skew (figure 6). The melanopsin suppression of the cone-directed wnERG amplitude was evident as a leftward shift of the frequency distributions (figure 6*a*). The melanopsin enhancement of the cone-directed wnVEP was evident as a rightward shift of the frequency distribution (figure 6*b*). The implicit times became progressively longer with transmission from the outer retinal cone photoreceptors (N1 = ~11 ms), bipolar cells (P1 = ~39 ms) to the parieto-occipital regions of the visual cortex (P2 = ~101 ms) (figure 6*c*), consistent with the expected event timings [58], but remained stable with the change in melanopsin excitation.

The signal to noise ratio of retinal ganglion cells is proportional to the luxotonic response of ipRGCs [59]. To determine whether the coding efficiency of the cone-pathway differs at a site prior to (i.e. the wnERG) and post-luxotonic ipRGC modulation of the cone signal (i.e. the wnVEP), we estimated the intra-observer variability across the 120 epochs for each observer by calculating the CoV for both amplitudes and implicit times (figure 6*a*,*b* insets). The CoV and signal to noise ratio are inversely related. The wnERG N1P1 amplitudes were significantly more variable with the higher melanopsin excitation (figure 6*a* inset; CoV: N1P1, $i_{low} = 47.74 \pm 3.90\%$, $i_{high} = 66.20 \pm 5.93\%$; $t_9 = 3.56$, $p = 0.01$), whereas the pattern was opposite for the cortical evoked wnVEP responses (figure 6*b*, inset); the variability in N2P2 amplitudes significantly decreased with the higher ($52.66 \pm 3.68\%$)

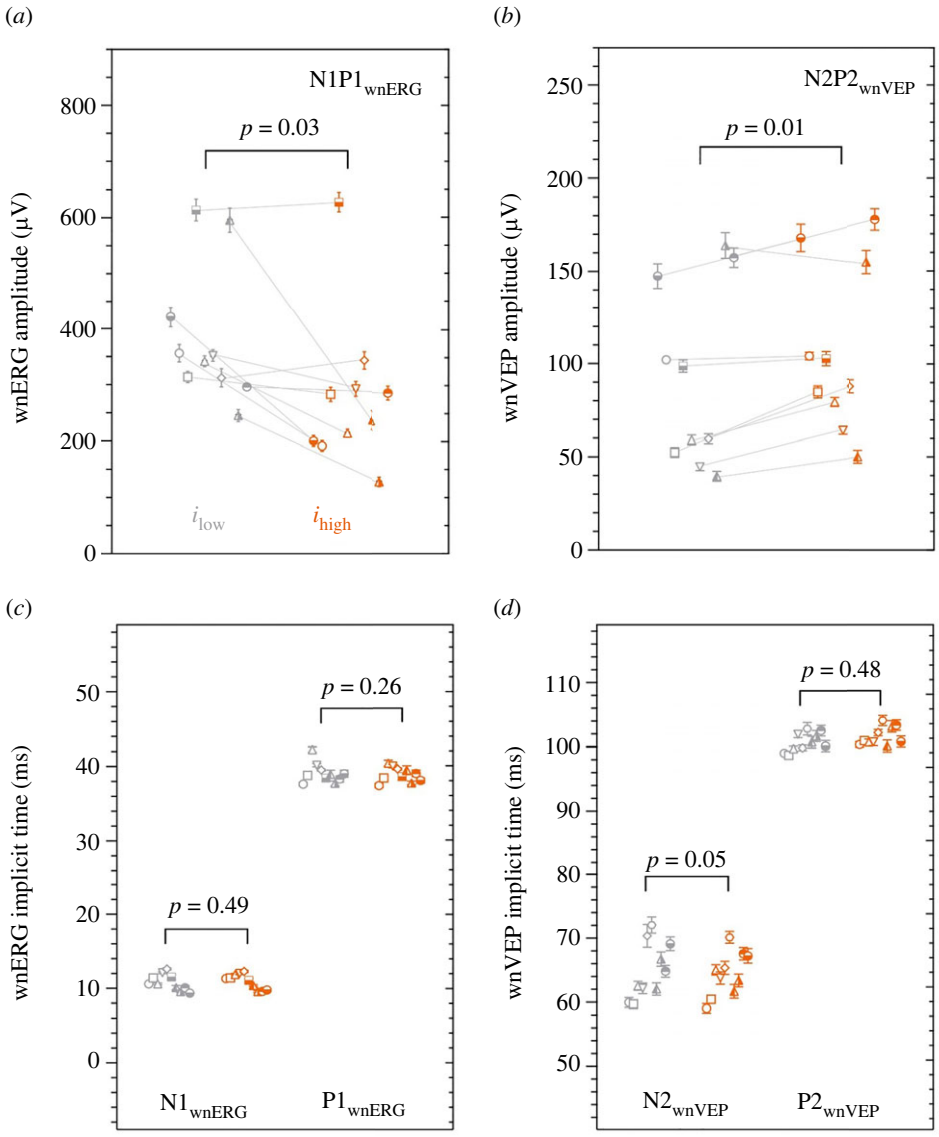

Figure 3. The cone-directed signals at the level of the retina (wnERG) and primary visual cortex (wnVEP). Each observer is represented by a unique symbol (mean ± s.e.m.); for each observer, the grey and orange symbols are connected by a grey line, indicating the transition from the low to high melanopsin excitation. (*a*) The N1P1 amplitudes of the cone-directed white noise electroretinogram (wnERG) measured under low melanopsin (grey symbols; i_{low}) or high melanopsin excitation (orange symbols; i_{high}) ($n = 10$). (*b*) N2P2 amplitudes for the cone-directed white noise visual evoked potential (wnVEP). (*c*) N1 and P1 implicit times for the wnERG. (*d*) N2 and P2 implicit times for the wnVEP.

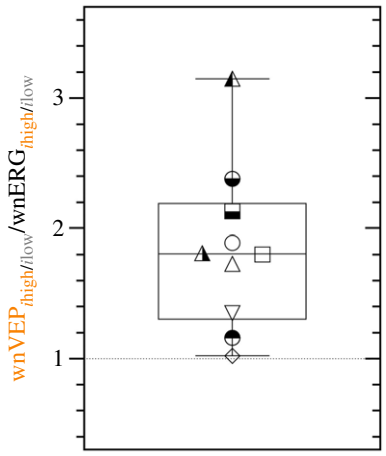

Figure 4. The wnVEP to wnERG amplitude ratio with higher (i_{high}) to lower (i_{low}) melanopsin excitation. Each observer is represented by a unique symbol ($n = 10$ observers). A ratio of < 1 indicates suppression and > 1 indicates amplification.

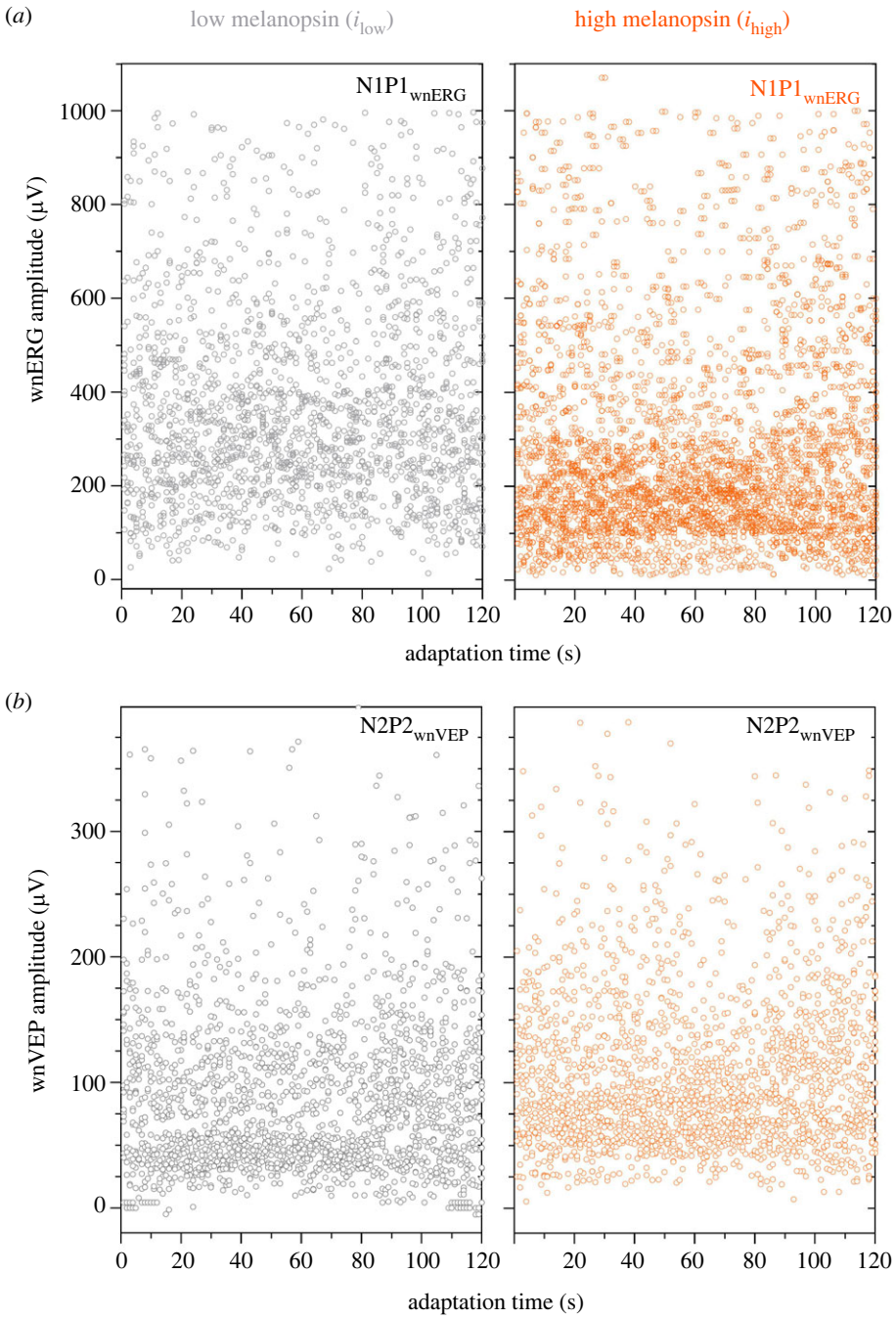

Figure 5. Short-term (2 min) stability of the cone-directed signals at the level of the retina (wnERG, upper panels) and primary visual cortex (wnVEP, lower panels). (*a*) The N1P1 amplitudes of the cone-directed white noise electroretinogram (wnERG) measured under low melanopsin (left panel, grey symbols; i_{low}) or high melanopsin excitation (right panel, orange symbols; i_{high}) plotted as a function of adaptation time for 10 observers (from a total of at least 1200 impulse response functions). (*b*) N2P2 amplitudes for the cone-directed white noise visual evoked potential (wnVEP).

than lower melanopsin excitation (60.13 ± 5.13%) ($t_9 = 2.98$, $p = 0.02$). To determine the co-variance between the melanopsin-mediated change in cone-directed wnERG or wnVEP amplitude and CoV as a measure of coding efficiency, we calculated the ratio of amplitude or CoV between the two melanopsin states. With increasing melanopsin excitation, the wnERG CoV increased 1.39-fold, mirroring the 1.37-fold corresponding decrease in the wnERG amplitude; also, the wnVEP CoV decreased by 1.12-fold, mirroring the 1.16-fold corresponding increase in the wnVEP amplitude. Intra-observer variability in the implicit times was invariant of the melanopsin excitation in the retina and brain as expected, given the similarity of the timings in the two conditions.

4. Discussion

By using photoreceptor silent substitution to precisely stabilize the rhodopsin activation under conditions of constant photometric luminance, the cortical evoked responses of the cone pathway were found to depend on the biological efficacy of the melanopsin excitation in the adapting light. A change in melanopsin excitation from low to high designed to capture elements of its total daytime variation modulated the amplitude of the cone-mediated visual pathway signal by 1.84× during transmission from the retina to the visual cortex. Cone signals that were initially supressed in the retina (N1P1 = –27%) were subsequently amplified when measured in the visual cortex (N2P2 = + 16%) with high melanopsin daylight conditions.

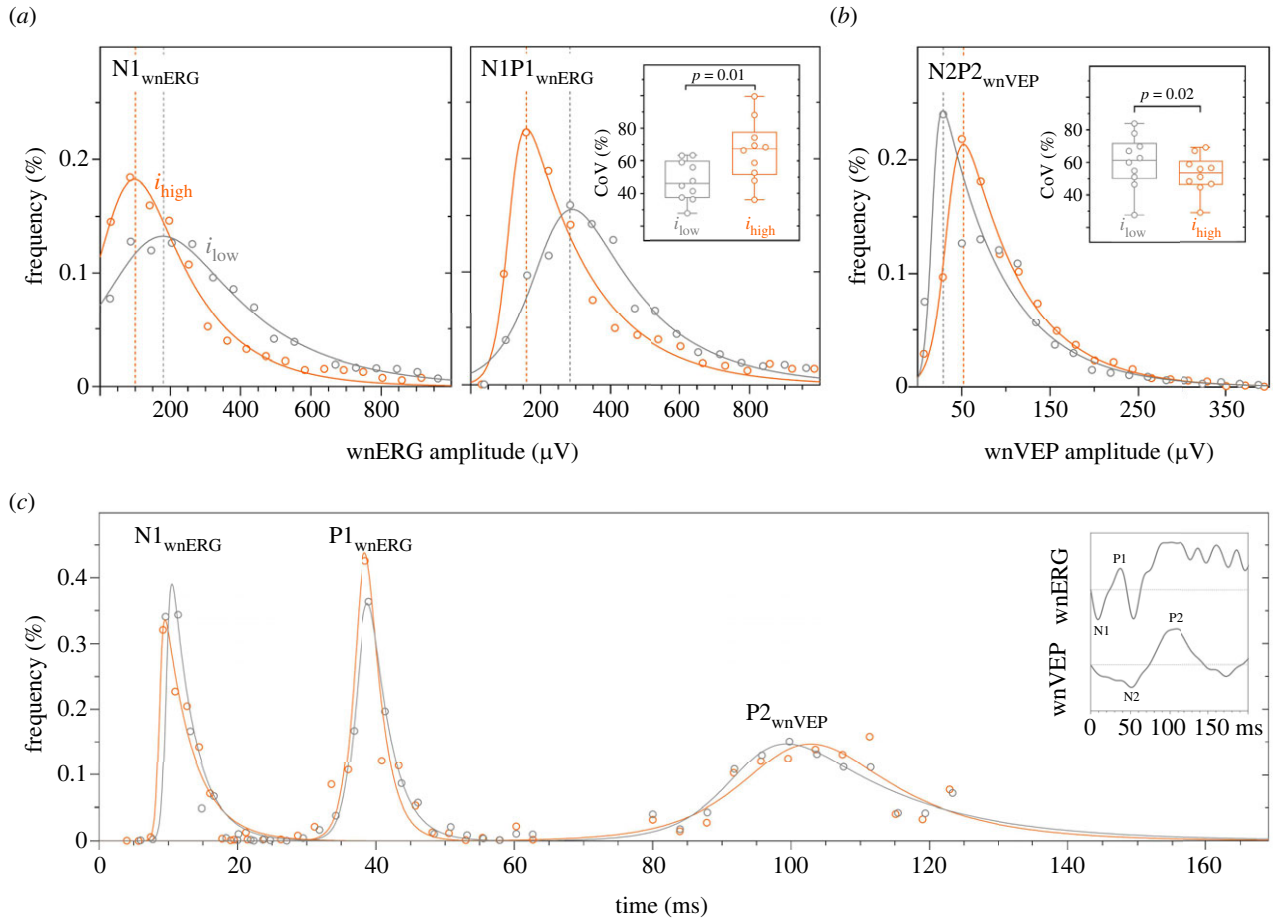

Figure 6. Effect of the biological efficacy of melanopsin on the amplitude (upper panels) and implicit time (lower panel) of cone signals measured at the level of the retina (wnERG) and primary visual cortex (wnVEP). (*a*) Frequency distributions of the cone-directed white noise electroretinogram (wnERG) measured under low melanopsin (i_{low}; grey circles and lines) and high melanopsin excitation (i_{high}; orange circles and lines). All observers ($n = 10$) and trials are analysed together (at least 1200 trials per condition). The solid lines are the best-fitting hyperbolic secant functions. Dotted vertical lines are the distribution modes. The inset (top middle panel) shows the intra-observer coefficient of variation (CoV) of the wnERG N1P1 amplitudes. (*b*) Visual evoked potential (wnVEP) amplitudes. The inset (top right panel) indicates the intra-observer coefficient of variation (CoV) of the wnVEP N2P2 amplitudes. (*c*) wnERG and VEP implicit times.

The suppression of the wnERG may signify action of melanopsin excitation-dependent gain control. In the retina, the detection of contrast over a wider dynamic range than the response of single cells depends on light adaptation to reduce the neuronal gain [60]. Because spatially antagonist centre-surround receptive fields only have indirect access to the ambient light level from luxotonic inputs via ipRGCs [1,61,62] and the graded output voltages from cones [63,64], the ipRGC signals may have a role in altering a cell's contrast response function by modulating gain within the inner retina, including between bipolar, amacrine and ganglion cells, which is a known location in primates for controlling the cone signal gain [65–68].

We observed that the cortical VEP is amplified with reference to the retinal ERG, and the amplitude dependence on the melanopsin excitation is reversed; what was attenuated in the outer retinal pathways represented in the ERG is amplified in the VEP. The adaptational response of the retina with the higher melanopsin excitation had a minor impact on the timing of the cortical evoked response, with the implicit times remaining stable during the short 2 min recording period at the level of retina and cortex (figure 5*c*). A relatively stable implicit time was not unexpected because melanopsin excitation suppresses the mouse flash ERG amplitude without affecting implicit time [40], and the b-wave implicit time does not change during 20 min adaptation [69]. In humans, the effect of melanopsin-dependent cone adaptation of the flash ERG manifests as faster (by 6–8 ms) b-wave implicit times only over longer time intervals from at least 15–120 min [11]. As determined from human behavioural estimates with photoreceptor directed light stimulation in reaction time [70], pupillometry [71,72], temporal summation [16] and subjective time expansion paradigms [73], in addition to cortical evoked potentials measured in melanopsin-only transgenic mice [74], the cone signals reach the brain before the melanopsin signal, in some conditions, by over 100 ms. The wnERG paradigm, which maintains the retina in a state of equilibrium more like natural viewing conditions than can a flash ERG, cannot temporally resolve these processes because the fast acting gain controls are operational within shorter timescales. For the flash ERG, the b-wave amplitudes are modulated by adaptation of the mass corneal potentials generated by cells in the inner nuclear layer [75,76], including feedback circuits from amacrines via interplexiform cells to horizontal cells [60,77,78], and such circuits are discussed later with reference to the melanopsin pathway. Taken together, melanopsin amplifies cortical responses without altering the signal transmission latency, indicating a role for melanopsin in optimizing the post-receptoral signal coding.

With increasing melanopsin excitation, the wnERG and VEP amplitudes exhibited an inverse covariance with variability. Cortical evoked responses have lower variability with higher melanopsin excitations (figure 6*b*, inset), indicative of increased signal to noise ratio for the same visual input, and therefore a subsequent increase in the amount of visual information that can be signalled

to the brain. Similarly, recordings in mice reveal that the tonic firing rate of retinal ganglion cells is scaled to the ambient irradiance by the luxotonic response of ipRGCs to increase the number of spikes available to convey visual information in daylight [79] and, at the level of the dLGN, the signal to noise ratio of cone responses is increased [59]. The melanopsin-dependent changes in gain can also modify the functional response of the mouse M4 ipRGC subtype involved in pattern vision [80]. An analogous amplification method is used in power distribution grids in the built environment to increase signal transmission efficiency, wherein electrical power lines transmit high voltages at low currents to minimize power loss over long distances [81]. We infer that this resultant increase in information flow to the visual cortex with higher melanopsin states has the effect in humans of optimizing the post-receptoral cone signal coding of retinal outputs, and provides a physiological correlate of the melanopsin-driven enhancement of cone-mediated contrast sensitivity [15,16,19]. The Weber fraction for cone-mediated vision therefore decreases with higher melanopsin excitations at the same photometric luminance [18], indicating that visual detection only requires a smaller increment in the stimulus magnitude. Given that VEP contrast responses are highly correlated with visual contrast thresholds [82–85], an implication of our VEP findings for vision is that the Weber fraction can be regulated by melanopsin at a site distal to retinal bipolar cells, and within the visual cortex.

The melanopsin-dependent adaptation observed in the cone ERG can be localized to cells within the inner nuclear layer in primates [76]. Here, the gain could be regulated by the balance between retrograde excitatory glutamatergic amacrine cells inputs between ipRGCs and ganglion cells, and the anterograde inhibitory inputs via VGlut3 amacrine cells [86]. Although undefined in primates, this inhibitory pathway does involve dopaminergic amacrine cells in mice [13,87]. The extensive connectivity of ipRGCs across all levels of the mouse retina supports their capacity to modify visual signalling at multiple loci. In addition to their effect on photoreceptor [88] and bipolar cell function [40], the amplification may involve excitatory glutamatergic amacrine cell feedback from ipRGCs to ganglion cells [86,89], through ipRGC axon collaterals to the inner plexiform layer [90] and/or via gap junctions to other ganglion cells [91,92]. At least 15 brain areas receive direct ipRGC projections to mediate the effects of light on visual and non-visual functions [93]. In macaques, a higher order cortico-geniculate feedback pathway could amplify the signal via excitatory glutamatergic feedback from cortical layer VI to the LGN in as little as 37 ms [94]. The amplification could involve the excitatory convergence of different retino-geniculate inputs on single cortical neurones [95,96]. Our inference is that independent, luxotonic ipRGC inputs to the LGN and/or higher visual areas can regulate this excitatory effect on the non-melanopsin pathway signals, but this is yet to be directly tested *in vivo*.

To maximize the effect size of the melanopsin state on cone signalling while controlling the rhodopsin excitation, we evaluated the largest range in melanopsin states our system could produce. With this experimental approach, we observe that melanopsin directly affects cone signals present in the visual cortex. Based on previous work [10], we anticipate the suppressive effect of melanopsin on the cone-directed ERG will increase with both higher melanopsin excitations and adaptation levels, as will the melanopsin enhancement of the cone VEP. However, as is the case for human vision [97], the presence of nonlinearities at the extreme contrasts and light levels still need to be explored.

The relative sensitivities of cone, rod and melanopsin pathways are set by the spectral power distribution of the prevailing light. To understand how melanopsin-cone photoreceptor interactions optimize daylight contrast sensitivity, we spectrally engineered the light to modulate melanopsin independently of cones while stabilizing the rod activity. Our description of a functional amplification effect on cortical evoked visual responses with a change in the daylight melanopsin excitation provides an alternate view for regulating human visual contrast sensitivity. Spectrally tuning all five photoreceptor excitations [27] might itself provide a more practical experimental paradigm to evaluate time-of-day circadian effects systematically and efficiently in a laboratory setting, and to study afferent pathway modulation of higher order processes. It will be interesting to determine how the retinal and cortical melanopsin pathways modulate light-dependent effects on visual function and other electrophysiological signals, such as the electroencephalogram [93,98]. Although photometric luminance is the primary metric used in industry to specify the visual effectiveness of a light [99], we show that cone-mediated vision is also dependent on the ambient spectral and irradiance content of the light that drives the luxotonic melanopsin signal [38], independent of the photometric luminance and rod excitation, which is critical because melanopsin-rod-cone interactions have non-complementary effects on visual contrast sensitivity.

Ethics. All experimental protocols were conducted in accordance with the institutional Human Research Ethics Committee approval (no. 1700000699) and followed the tenets of the Declaration of Helsinki.

Data accessibility. Data are available from the Dryad Digital Repository [100].

Authors' contributions. P.A.: conceptualization, data curation, formal analysis, investigation, methodology, writing—original draft, writing—review and editing; S.U.: conceptualization, data curation, formal analysis, investigation, methodology, writing—review and editing; B.F.: conceptualization, data curation, formal analysis, investigation, methodology, resources, supervision, writing—original draft, writing—review and editing; A.J.Z.: conceptualization, data curation, formal analysis, funding acquisition, investigation, methodology, project administration, resources, supervision, writing—original draft, writing—review and editing.

All authors gave final approval for publication and agreed to be held accountable for the work performed therein.

Conflict of interest declaration. We declare we have no competing interests.

Funding. Supported by an Australian Research Council Future Fellowship ARC-FT180100458 (A.J.Z.).

Acknowledgements. We thank Thomas W. Nugent and Drew D. Carter for technical development support.

References

1. Dacey DM *et al.* 2005 Melanopsin-expressing ganglion cells in primate retina signal colour and irradiance and project to the LGN. *Nature* **433**, 749–754. (doi:10.1038/nature03387)
2. Hannibal J, Kankipati L, Strang CE, Peterson BB, Dacey D, Gamlin PD. 2014 Central projections of intrinsically photosensitive retinal ganglion cells in the macaque monkey. *J. Comp. Neurol.* **522**, 2231–2248. (doi:10.1002/cne.23555)

3. Spitschan M, Bock AS, Ryan J, Frazzetta G, Brainard DH, Aguirre GK. 2017 The human visual cortex response to melanopsin-directed stimulation is accompanied by a distinct perceptual experience. *Proc. Natl Acad. Sci. USA* **114**, 12 291–12 296. (doi:10.1073/pnas.1711522114)
4. Cao D, Chang A, Gai S. 2018 Evidence for an impact of melanopsin activation on unique white perception. *J. Opt. Soc. Am. A* **35**, B287–B291. (doi:10.1364/JOSAA.35.00B287)
5. Zele AJ, Feigl B, Adhikari P, Maynard ML, Cao D. 2018 Melanopsin photoreception contributes to human visual detection, temporal and colour processing. *Sci. Rep.* **8**, 3842. (doi:10.1038/s41598-018-22197-w)
6. DeLawyer T, Tsujimura S, Shinomori K. 2020 Relative contributions of melanopsin to brightness discrimination when hue and luminance also vary. *J. Opt. Soc. Am. A* **37**, A81–AA8. (doi:10.1364/JOSAA.382349)
7. Horiguchi H, Winawer J, Dougherty RF, Wandell BA. 2013 Human trichromacy revisited. *Proc. Natl Acad. Sci. USA* **110**, E260–E329.
8. Brown TM, Tsujimura S, Allen AE, Wynne J, Bedford R, Vickery G, Vugler A, Lucas RJ. 2012 Melanopsin-based brightness discrimination in mice and humans. *Curr. Biol.* **22**, 1134–1141. (doi:10.1016/j.cub.2012.04.039)
9. Zele AJ, Adhikari P, Feigl B, Cao D. 2018 Cone and melanopsin contributions to human brightness estimation. *J. Opt. Soc. Am. A.* **35**, B19–B25. (doi:10.1364/JOSAA.35.000B19)
10. Adhikari P, Zele AJ, Cao D, Kremers J, Feigl B. 2019 The melanopsin-directed white noise electroretinogram (wnERG). *Vision Res.* **164**, 83–93. (doi:10.1016/j.visres.2019.08.007)
11. Hankins M, Lucas R. 2002 The primary visual pathway in humans is regulated according to long-term light exposure through the action of a nonclassical photopigment. *Curr. Biol.* **12**, 191–198. (doi:10.1016/S0960-9822(02)00659-0)
12. Barnard AR, Hattar S, Hankins MW, Lucas RJ. 2006 Melanopsin regulates visual processing in the mouse retina. *Curr. Biol.* **16**, 389–395. (doi:10.1016/j.cub.2005.12.045)
13. Zhang DQ, Belenky MA, Sollars PJ, Pickard GE, McMahon DG. 2012 Melanopsin mediates retrograde visual signaling in the retina. *PLoS ONE* **7**, e42647. (doi:10.1371/journal.pone.0042647)
14. Zhang DQ, Wong KY, Sollars PJ, Berson DM, Pickard GE, McMahon DG. 2008 Intraretinal signaling by ganglion cell photoreceptors to dopaminergic amacrine neurons. *Proc. Natl Acad. Sci. USA* **105**, 14 181–14 186. (doi:10.1073/pnas.0803893105)
15. Chien SE, Yeh SL, Yamashita W, Tsujimura SI. 2023 Enhanced human contrast sensitivity with increased stimulation of melanopsin in intrinsically photosensitive retinal ganglion cells. *Vision Res.* **209**, 108271. (doi:10.1016/j.visres.2023.108271)
16. Uprety S, Adhikari P, Feigl B, Zele AJ. 2022 Melanopsin photoreception differentially modulates rod-and cone-mediated human temporal vision. *iScience* **25**, 104529. (doi:10.1016/j.isci.2022.104529)
17. Fukuda Y, Higuchi S, Yasukouchi A, Morita T. 2012 Distinct responses of cones and melanopsin-expressing retinal ganglion cells in the human electroretinogram. *J. Physiol. Anthropol.* **31**, 20. (doi:10.1186/1880-6805-31-20)
18. Vincent J, Haggerty EB, Brainard DH, Aguirre GK. 2021 Melanopic stimulation does not alter psychophysical threshold sensitivity for luminance flicker. *Sci. Rep.* **11**, 1–15. (doi:10.1038/s41598-020-79139-8)
19. Zele AJ, Adhikari P, Cao D, Feigl B. 2019 Melanopsin driven enhancement of cone-mediated visual processing. *Vision Res.* **160**, 72–81. (doi:10.1016/j.visres.2019.04.009)
20. Frederiksen R, Morshedian A, Tripathy SA, Xu T, Travis GH, Fain GL, Sampath AP. 2021 Rod photoreceptors avoid saturation in bright light by the movement of the G protein transducin. *J. Neurosci.* **41**, 3320–3330. (doi:10.1523/JNEUROSCI.2817-20.2021)
21. Tikidji-Hamburyan A *et al.* 2017 Rods progressively escape saturation to drive visual responses in daylight conditions. *Nat. Commun.* **8**, 1813. (doi:10.1038/s41467-017-01816-6)
22. Borghuis BG, Ratliff CP, Smith RG. 2018 Impact of light-adaptive mechanisms on mammalian retinal visual encoding at high light levels. *J. Neurophysiol.* **119**, 1437–1449. (doi:10.1152/jn.00682.2017)
23. Yin L, Smith RG, Sterling P, Brainard DH. 2006 Chromatic properties of horizontal and ganglion cell responses follow a dual gradient in cone opsin expression. *J. Neurosci.* **26**, 12 351–12 361. (doi:10.1523/JNEUROSCI.1071-06.2006)
24. Kremers J, Czop D, Link B. 2009 Rod and S-cone driven ERG signals at high retinal illuminances. *Doc Ophthalmol.* **118**, 205–216. (doi:10.1007/s10633-008-9159-0)
25. Adhikari P, Carter DD, Feigl B, Zele AJ. 2022 Design and validation of a chart-based measure of the limits of spatial contrast sensitivity. *Ophthalmic Physiol. Opt.* **42**, 110–122. (doi:10.1111/opo.12914)
26. Estevez O, Spekreijse H. 1982 The 'silent substitution' method in visual research. *Vision Res.* **22**, 681–691. (doi:10.1016/0042-6989(82)90104-3)
27. Nugent TW, Carter DD, Uprety S, Adhikari P, Feigl B, Zele AJ. 2023 Protocol for isolation of melanopsin and rhodopsin in the human eye using silent substitution. *iScience*.
28. Nugent TW, Zele AJ. 2022 A five-primary Maxwellian-view display for independent control of melanopsin, rhodopsin, and three-cone opsins on a fine spatial scale. *J. Vis.* **22**, 20. (doi:10.1167/jov.22.12.20)
29. Odom JV *et al*. 2016 ISCEV standard for clinical visual evoked potentials: (2016 update). *Doc Ophthalmol.* **133**, 1–9. (doi:10.1007/s10633-016-9553-y)
30. Enezi J, Revell V, Brown T, Wynne J, Schlangen L, Lucas R. 2011 A 'melanopic' spectral efficiency function predicts the sensitivity of melanopsin photoreceptors to polychromatic lights. *J. Biol. Rhythms.* **26**, 314–323. (doi:10.1177/0748730411409719)
31. Barrionuevo PA, Cao D. 2014 Contributions of rhodopsin, cone opsins, and melanopsin to postreceptoral pathways inferred from natural image statistics. *J. Opt. Soc. Am. A.* **31**, A131–A139. (doi:10.1364/JOSAA.31.00A131)
32. Evéquoz G, Truffer F, Geiser M. 2021 Maximum possible contrast level for silent substitution: a theoretical model applied to melanopsin stimulation. *J. Opt. Soc. Am. A* **38**, 1312–1319. (doi:10.1364/JOSAA.420373)
33. Uprety S, Zele AJ, Feigl B, Cao D, Adhikari P. 2021 Optimizing methods to isolate melanopsin-directed responses. *J. Opt. Soc. Am. A.* **38**, 1051–1064. (doi:10.1364/JOSAA.423343)
34. Feigl B, Carter DD, Zele AJ. 2023 Photoreceptor enhanced light therapy (PELT): a framework for implementing biologically directed integrative lighting. *J. Leukos.* **19**, 294–307. (doi:10.1080/15502724.2022.2123816)
35. Pant M, Zele AJ, Feigl B, Adhikari P. 2021 Light adaptation characteristics of melanopsin. *Vision Res.* **188**, 126–138. (doi:10.1016/j.visres.2021.07.005)
36. Hathibelagal AR, Feigl B, Kremers J, Zele AJ. 2016 Correlated and uncorrelated invisible temporal white noise alters mesopic rod signaling. *J. Opt. Soc. Am. A* **33**, A93–103. (doi:10.1364/JOSAA.33.000A93)
37. Zele AJ, Feigl B, Kambhampati PK, Aher A, McKeefry D, Parry N, Maguire J, Murray I, Kremers J. 2017 A temporal white noise analysis for extracting the impulse response function of the human electroretinogram. *Transl. Vis. Sci. Technol.* **6**, 1. (doi:10.1167/tvst.6.6.1)
38. CIE. 2018 *CIE system for metrology of optical radiation for ipRGC-influenced responses to light CIE DIS 026/E:2018*. Vienna, Austria: Commission Internationale de l'Éclairage.
39. Spitschan M, Aguirre GK, Brainard DH. 2015 Selective stimulation of penumbral cones reveals perception in the shadow of retinal blood vessels. *PLoS ONE* **10**, e0124328. (doi:10.1371/journal.pone.0124328)
40. Allen AE, Storchi R, Martial FP, Petersen RS, Montemurro MA, Brown TM, Lucas RJ. 2014 Melanopsin-driven light adaptation in mouse vision. *Curr. Biol.* **24**, 2481–2490. (doi:10.1016/j.cub.2014.09.015)

41. Langheinrich T, Tebartz van Elst L, Lagreze WA, Bach M, Lucking CH, Greenlee MW. 2000 Visual contrast response functions in Parkinson's disease: evidence from electroretinograms, visually evoked potentials and psychophysics. *Clin. Neurophysiol.* **111**, 66–74. (doi:10.1016/S1388-2457(99)00223-0)
42. Pangeni G, Horn FK, Kremers J. 2010 A new interpretation of components in the ERG signals to sine wave luminance stimuli at different temporal frequencies and contrasts. *J. Vis. Neurosc.* **27**, 79–90. (doi:10.1017/S0952523810000179)
43. Hess RF, Baker Jr CL. 1984 Human pattern-evoked electroretinogram. *J. Neurophysiol.* **51**, 939–951. (doi:10.1152/jn.1984.51.5.939)
44. Maxwell JC. 1856 On the unequal sensibility of the Foramen Centrale to light of different colours. *Athenaeum* **1505**, 1093.
45. Gardasevic M, Lucas RJ, Allen AE. 2019 Appearance of Maxwell's spot in images rendered using a cyan primary. *Vision Res.* **165**, 72–79. (doi:10.1016/j.visres.2019.10.004)
46. Trezona P. 1973 The tetrachromatic colour match as a colorimetric technique. *Vision Res.* **13**, 9–25. (doi:10.1016/0042-6989(73)90161-2)
47. McCulloch DL *et al.* 2015 ISCEV standard for full-field clinical electroretinography (2015 update). *Doc Ophthalmol.* **130**, 1–12. (doi:10.1007/s10633-014-9473-7)
48. Kremers J, Aher AJ, Parry NRA, Patel NB, Frishman LJ. 2022 Electroretinographic responses to luminance and cone-isolating white noise stimuli in macaques. *Front. Neurosci.* **16**, 925405. (doi:10.3389/fnins.2022.925405)
49. Stallwitz N, Joachimsthaler A, Kremers J. 2022 Luminance white noise electroretinograms (wnERGs) in mice. *Front. Neurosci.* **16**, 1075126. (doi:10.3389/fnins.2022.1075126)
50. Zele AJ, Feigl B, Kambhampati PK, Hathibelagal AR, Kremers J. 2015 A method for estimating intrinsic noise in electroretinographic (ERG) signals. *Doc. Ophthalmol.* **131**, 85–94. (doi:10.1007/s10633-015-9510-1)
51. Abboud S, Sadeh D. 1984 The use of cross-correlation function for the alignment of ECG waveforms and rejection of extrasystoles. *Comput. Biomed. Res.* **17**, 258–266. (doi:10.1016/S0010-4809(84)80017-8)
52. Rhudy M, Bucci B, Vipperman J, Allanach J, Abraham B (eds). 2010 Microphone array analysis methods using cross-correlations. In *Proceedings of the ASME International Mechanical Engineering Congress and Exposition 2009, Lake Buena Vista, FL, 13–19 November 2009*, pp. 281–288. Houston, TX: American Society of Mechanical Engineers.
53. Adhikari P, Zele AJ, Feigl B. 2015 The post-illumination pupil response (PIPR). *Invest. Ophthalmol. Vis. Sci.* **56**, 3838–3849. (doi:10.1167/iovs.14-16233)
54. Zele AJ, Feigl B, Smith SS, Markwell EL. 2011 The circadian response of intrinsically photosensitive retinal ganglion cells. *PLoS ONE* **6**, e17860. (doi:10.1371/journal.pone.0017860)
55. Kraut MA, Arezzo JC, Vaughan Jr HG. 1985 Intracortical generators of the flash VEP in monkeys. *Electroencephalogr. Clin. Neurophysiol.* **62**, 300–312. (doi:10.1016/0168-5597(85)90007-3)
56. Di Russo F, Martinez A, Sereno MI, Pitzalis S, Hillyard SA. 2002 Cortical sources of the early components of the visual evoked potential. *Hum. Brain Mapp.* **15**, 95–111. (doi:10.1002/hbm.10010)
57. Scott DW. 1979 On optimal and data-based histograms. *Biometrika* **66**, 605–610. (doi:10.1093/biomet/66.3.605)
58. Omoto S *et al.* 2010 P1 and P2 components of human visual evoked potentials are modulated by depth perception of 3-dimensional images. *Clin. Neurophysiol.* **121**, 386–391. (doi:10.1016/j.clinph.2009.12.005)
59. Storchi R *et al.* 2015 Melanopsin-driven increases in maintained activity enhance thalamic visual response reliability across a simulated dawn. *Proc. Natl Acad. Sci. USA* **112**, E5734–E5743. (doi:10.1073/pnas.1505274112)
60. Shapley R, Enroth-Cugell C. 1984 Visual adaptation and retinal gain controls. *Prog. Retin. Eye Res.* **3**, 263–346. (doi:10.1016/0278-4327(84)90011-7)
61. Kayama Y, Riso RR, Bartlett JR, Doty RW. 1979 Luxotonic responses of units in macaque striate cortex. *J. Neurophysiol.* **42**, 1495–1517. (doi:10.1152/jn.1979.42.6.1495)
62. Kinoshita M, Komatsu H. 2001 Neural representation of the luminance and brightness of a uniform surface in the macaque primary visual cortex. *J. Neurophysiol.* **86**, 2559–2570. (doi:10.1152/jn.2001.86.5.2559)
63. Baden T, Berens P, Bethge M, Euler T. 2013 Spikes in mammalian bipolar cells support temporal layering of the inner retina. *Curr. Biol.* **23**, 48–52. (doi:10.1016/j.cub.2012.11.006)
64. Normann RA, Perlman I. 1979 The effects of background illumination on the photoresponses of red and green cones. *J. Physiol.* **286**, 491–507. (doi:10.1113/jphysiol.1979.sp012633)
65. Dunn FA, Lankheet MJ, Rieke F. 2007 Light adaptation in cone vision involves switching between receptor and post-receptor sites. *Nature* **449**, 603–U12. (doi:10.1038/nature06150)
66. Purpura K, Tranchina D, Kaplan E, Shapley RM. 1990 Light adaptation in the primate retina: analysis of changes in gain and dynamics of monkey retinal ganglion cells. *Vis. Neurosci.* **4**, 75–93. (doi:10.1017/S0952523800002789)
67. Schnapf JL, Baylor DA. 1987 How photoreceptor cells respond to light. *Sci. Am.* **256**, 40–47. (doi:10.1038/scientificamerican0487-40)
68. Smith VC, Pokorny J, Lee BB, Dacey DM. 2008 Sequential processing in vision: the interaction of sensitivity regulation and temporal dynamics. *Vision Res.* **48**, 2649–2656. (doi:10.1016/j.visres.2008.05.002)
69. Prigge CL *et al.* 2016 M1 ipRGCs influence visual function through retrograde signaling in the retina. *J. Neurosci.* **36**, 7184–7197. (doi:10.1523/JNEUROSCI.3500-15.2016)
70. Gnyawali S, Feigl B, Adhikari P, Zele AJ. 2022 The role of melanopsin photoreception on visual attention linked pupil responses. *Eur. J. Neurosci.* **55**, 1986–2002. (doi:10.1111/ejn.15659)
71. Zele AJ, Adhikari P, Cao D, Feigl B. 2019 Melanopsin and cone photoreceptor inputs to the afferent pupil light response. *Front. Neurol.* **10**, 529. (doi:10.3389/fneur.2019.00529)
72. Tsujimura S, Tokuda Y. 2011 Delayed response of human melanopsin retinal ganglion cells on the pupillary light reflex. *Ophthalmic Physiol. Opt.* **31**, 469–479. (doi:10.1111/j.1475-1313.2011.00846.x)
73. Yang PL, Tsujimura SI, Matsumoto A, Yamashita W, Yeh SL. 2018 Subjective time expansion with increased stimulation of intrinsically photosensitive retinal ganglion cells. *Sci. Rep.* **8**, 11693. (doi:10.1038/s41598-018-29613-1)
74. Flood MD, Veloz HLB, Hattar S, Carvalho-de-Souza JL. 2022 Robust visual cortex evoked potentials (VEP) in Gnat1 and Gnat2 knockout mice. *Front. Cell Neurosci.* **16**, 654. (doi:10.3389/fncel.2022.1090037)
75. Grunert U, Jusuf PR, Lee SCS, Nguyen DT. 2011 Bipolar input to melanopsin containing ganglion cells in primate retina. *Vis. Neurosci.* **28**, 39–50. (doi:10.1017/S095252381000026X)
76. Masri RA, Weltzien F, Purushothuman S, Lee SCS, Martin PR, Grunert U. 2021 Composition of the inner nuclear layer in human retina. *Invest. Ophthalmol. Vis. Sci.* **62**, 22. (doi:10.1167/iovs.62.9.22)
77. Hood DC. 1990 The ERG and sites and mechanisms of retinal disease, adaptation, and development. In *Advances in photoreception: proceedings of a symposium on frontiers of visual science* (ed. National Research Council), pp. 41–58. Washington, DC: National Academic Press.
78. Wilson HR. 1997 A neural model of foveal light adaptation and afterimage formation1. *Vis. Neurosci.* **14**, 403–423. (doi:10.1017/S0952523800012098)
79. Milosavljevic N, Storchi R, Eleftheriou CG, Colins A, Petersen RS, Lucas RJ. 2018 Photoreceptive retinal ganglion cells control the information rate of the optic nerve. *Proc. Natl Acad. Sci. USA* **115**, E11817–E11826. (doi:10.1073/pnas.1810701115)

80. Sonoda T, Lee SK, Birnbaumer L, Schmidt TM. 2018 Melanopsin phototransduction Is repurposed by ipRGC subtypes to shape the function of distinct visual circuits. *Neuron* **99**, 754. (doi:10.1016/j.neuron.2018.06.032)
81. Guarnieri M. 2013 The beginning of electric energy transmission: part one [Historical]. *IEEE Ind. Electron. Mag.* **0**, 50–52. (doi:10.1109/MIE.2012.2236484)
82. Allen D, Norcia AM, Tyler CW. 1986 Comparative study of electrophysiological and psychophysical measurement of the contrast sensitivity function in humans. *Am. J. Optom. Physiol. Opt.* **63**, 442–449. (doi:10.1097/00006324-198606000-00008)
83. Cannon Jr MW. 1983 Contrast sensitivity: psychophysical and evoked potential methods compared. *Vision Res.* **23**, 87–95. (doi:10.1016/0042-6989(83)90045-7)
84. Seiple W, Kupersmith MJ, Holopigian K. 1995 Comparison of visual evoked potential and psychophysical contrast sensitivity. *Int. J. Neurosci.* **80**, 173–180. (doi:10.3109/00207459508986099)
85. Souza GS, Gomes BD, Saito CA, da Silva Filho M, Silveira LC. 2007 Spatial luminance contrast sensitivity measured with transient VEP: comparison with psychophysics and evidence of multiple mechanisms. *Invest. Ophthalmol. Vis. Sci.* **48**, 3396–3404. (doi:10.1167/iovs.07-0018)
86. Marshak DW *et al.* 2015 Synaptic connections of amacrine cells containing vesicular glutamate transporter 3 in baboon retinas. *Vis. Neurosci.* **32**, E006. (doi:10.1017/S0952523815000036)
87. Newkirk GS, Hoon M, Wong RO, Detwiler PB. 2013 Inhibitory inputs tune the light response properties of dopaminergic amacrine cells in mouse retina. *J. Neurophysiol.* **110**, 536–552. (doi:10.1152/jn.00118.2013)
88. Milosavljevic N, Cehajic-Kapetanovic J, Procyk CA, Lucas RJ. 2016 Chemogenetic activation of melanopsin retinal ganglion cells induces signatures of arousal and/or anxiety in mice. *Curr. Biol.* **26**, 2358–2363. (doi:10.1016/j.cub.2016.06.057)
89. Patterson SS, Kuchenbecker JA, Anderson JR, Neitz M, Neitz J. 2020 A color vision circuit for non-image-forming vision in the primate retina. *Curr. Biol.* **30**, 1269–1274. (doi:10.1016/j.cub.2020.01.040)
90. Joo HR, Peterson BB, Dacey DM, Hattar S, Chen SK. 2013 Recurrent axon collaterals of intrinsically photosensitive retinal ganglion cells. *Vis. Neurosci.* **30**, 175–182. (doi:10.1017/S0952523813000199)
91. Reifler AN *et al*. 2015 All spiking, sustained ON displaced amacrine cells receive gap-junction input from melanopsin ganglion cells. *Curr. Biol.* **25**, 2763–2773. (doi:10.1016/j.cub.2015.09.018)
92. Müller LP, Do MTH, Yau KW, He S, Baldridge WH. 2010 Tracer coupling of intrinsically photosensitive retinal ganglion cells to amacrine cells in the mouse retina. *J. Comp. Neurol.* **518**, 4813–4824. (doi:10.1002/cne.22490)
93. Joyce DS, Houser KW, Peirson SN, Zeitzer JM, Zele AJ. 2022 *Melanopsin vision: sensation and perception through intrinsically photosensitive retinal ganglion cells*. Cambridge, UK: Cambridge University Press.
94. Briggs F, Usrey WM. 2007 A fast, reciprocal pathway between the lateral geniculate nucleus and visual cortex in the macaque monkey. *J. Neurosci.* **27**, 5431–5436. (doi:10.1523/JNEUROSCI.1035-07.2007)
95. Dreher B, Wang C, Burke W. 1996 Limits of parallel processing: Excitatory convergence of different information channels on single neurons in striate and extrastriate visual cortices. *Clin. Exp. Pharmacol. Physiol.* **23**, 913–925. (doi:10.1111/j.1440-1681.1996.tb01143.x)
96. Zeki S, Shipp S. 1988 The functional logic of cortical connections. *Nature* **335**, 311–317. (doi:10.1038/335311a0)
97. Blackwell HR. 1946 Contrast thresholds of the human eye. *J. Am. Opt. Soc. A* **36**, 624–643. (doi:10.1364/JOSA.36.000624)
98. Souman JL, Tinga AM, Te Pas SF, van Ee R, Vlaskamp BNS. 2018 Acute alerting effects of light: a systematic literature review. *Behav. Brain Res.* **337**, 228–239. (doi:10.1016/j.bbr.2017.09.016)
99. CIE. 1994 *Light as a true visual quantity: principles of measurement*. Paris, France: Bureau Central de la CIE.
100. Adhikari P, Uprety S, Feigl B, Zele AJ. 2024 Melanopsin-mediated amplification of cone signals in the human visual cortex [Dataset]. Dryad Digital Repository. (doi:10.5061/dryad.12jm63z62)